Green Chemistry

PAPER

View Article Online
View Journal | View Issue

Cite this: *Green Chem.*, 2022, **24**, 3723

Electric potential-determined redox intermediates for effective recycling of spent lithium-ion batteries†

Yunhui Hua,‡[a,b] Zhenghe Xu,[c] Baojun Zhao[b,d] and Zuotai Zhang *[a]

Received 24th January 2022,
Accepted 29th March 2022

DOI: 10.1039/d2gc00331g

rsc.li/greenchem

Recycling of spent lithium-ion batteries (LIBs) by hydrometallurgy faces a major problem of consuming an excessive amount of acid and requiring different redox additives for effective metal leaching. Reducing chemical consumption in the recycling process is highly desirable for the environmentally friendly and sustainable development of renewable energy. In this study, an electrochemical approach for analyzing electric potentials was developed to evaluate redox abilities. Based on the results, a salt leaching method was proposed using water-soluble $NH_4Fe(SO_4)_2$ as a redox intermediate for synergistic recovery of valuable metals from spent ternary lithium-ion batteries (NCM) and $LiFePO_4$ batteries (LFP). More than 97% of the Li, Mn, Co and Ni from the mixed cathode can be leached under mild conditions (50 °C, 30 min), with PO_4^{3-} being completely retained in residues. The first-step reaction between Fe^{3+} and LFP to release Fe^{2+} proceeded rapidly, whereas the following slower reaction between Fe^{2+} and NCM was the rate-controlling process. Thermodynamic analysis of leaching solutions was carried out systematically and shown to be feasible for designing a precipitate recovery process for both LFP and NCM battery systems, with the recovered products being used for regenerating new materials. The synergistic salt-leaching treatment of spent LFP and NCM batteries based on electrochemical principles helped achieve high efficiency and high selectivity with a great benefit to preserving the environment.

1 Introduction

A global tendency toward sustainable development is leading to a rapid increase in applications of mobile equipment, including electric vehicles (EVs) and other portable electronic devices. According to statistics from international agencies, the annual sales of EVs in 2021 still reached a growth of 98% over 2020 despite the worldwide impact of the COVID-19 pandemic.[1,2] More countries are setting carbon-neutral policies and more electric transportation modes are expected in the future. Electric transportation mostly utilizes lithium-ion batteries (LIBs) as a power source because of their superior performance to those of lead, Ni–Cd, and Ni–MH batteries.[3,4] However, after their life span, large amounts of spent batteries are generated, with the associated environmental pollution in the form of heavy metals and toxic organics.[5,6] On the one hand, spent LIBs still have relatively high energy potential and may be able to go through second life, which may extend their lifetimes. The comprehensive use of spent LIBs can also reduce the environmental pressure by providing flexibility and additional time to establish the required recycling facilities for sustainable development.[7] Spent LIBs that finally reach the end of their lifetime contain a high content of valuable metals such as Co, Ni and Li, which can be an important resource for sustainable production.[8,9] Therefore, recycling of spent LIBs is of great importance from both economic and environmental perspectives.

Most research on recycling of spent LIBs focuses on the recovery of valuable metals from cathodes, including $LiCoO_2$ (LCO), $LiNi_xCo_yMn_zO_2$ (NCM), $LiNi_xCo_yAl_zO_2$ (NCA), $LiMn_2O_4$ (LMO) and $LiFePO_4$ (LFP).[10] As for LCO, NCM, NCA and LMO, these cathode materials are usually composed of high-valence, transition metal oxides. The methods to recover these valuable transition metals are primarily pyrometallurgy and hydrometallurgy, while other methods including direct recycling are still in early stages of development.[11] Pyrometallurgy uses a

[a]*School of Environmental Science and Engineering, Southern University of Science and Technology (SUSTech), Shenzhen 518055, China.*
E-mail: zhangzt@sustech.edu.cn
[b]*School of Chemical Engineering, The University of Queensland, St Lucia 4072, Brisbane, Australia*
[c]*Department of Materials Science and Engineering, Southern University of Science and Technology (SUSTech), Shenzhen 518055, China*
[d]*Faculty of Materials, Metallurgy and Chemistry, Jiangxi University of Science and Technology, Ganzhou 341000, China*

†Electronic supplementary information (ESI) available: Fig. S1–S12. See DOI: https://doi.org/10.1039/d2gc00331g

‡First author of the article.

carbothermic reduction or salt-roasting method at high temperatures to extract metals, which requires high energy consumption and generates greenhouse gases, toxic gases and other hazardous slags.[12,13] The pyrometallurgical process therefore could impose a number of environmental risks including global warming and photochemical pollution.[14] To attain the energy-saving and carbon-neutral objective for future development, hydrometallurgy is becoming more preferable.[15] Hydrometallurgy uses inorganic acids (*e.g.*, HCl[16,17] and H_2SO_4 [18,19]) or organic acids (*e.g.*, acetic acid,[20] citric acid,[21–23] and oxalic acid[24,25]) as leaching agents for metal recovery. However, various kinds of spent battery cathodes need to be separated first because they require different redox additives for metal recovery. For the spent NCM and LCO cathodes, for example, reductants (*e.g.*, H_2O_2, $NaHSO_3$, and ascorbic acid[26–28]) are usually used to facilitate the reduction and release of the metals; but for spent LFP cathodes, additional oxidants (*e.g.*, H_2O_2 and $Na_2S_2O_8$) are required to release Li for recovery.[29,30] Moreover, excessive amounts of leaching reagents are often needed to achieve high leaching efficiency because some components, such as H_2O_2 in the reagent, are unstable and easily decomposed by the catalytic effect of the metal ions (*e.g.*, Fe^{3+}/Fe^{2+} (ref. 31 and 32)). It is desirable to investigate new processes to reduce the use of reductant and oxidant additives to achieve green and highly efficient recycling of spent LIBs.[33]

To save energy and resources, some studies have proposed "treating waste by waste". For example, carbon black or aluminum foil from spent LIBs have been taken as reductants for spent LCO or NCM cathodes.[34,35] Spent Ni–MH batteries have also been reported as reductants for LCO cathodes, and valuable metals from both batteries can be effectively recovered.[36] LFP and NCM batteries have emerged as major battery types on the market and they are expected to occupy a greater market share in the future.[37] Some studies have attempted to use sulfuric acid to recycle LFP, LCO and NCM synergistically.[38,39] It was reported that the intrinsic redox reaction could limit the acid dosage and also reduce the addition of reductants or oxidants. However, the kinetics and mechanisms of the synergistic reactions remain unclear, and an in-depth study is needed to achieve efficient production. Moreover, sulfuric acid as a leaching agent does not have selectivity for every element. The phosphorus existing as PO_4^{3-} (or H_3PO_4, $H_2PO_4^-$, or HPO_4^{2-}) in the leaching solution will inevitably bring impurities into an NCM or LCO system, and the iron from LFP may not be able to combine with PO_4^{3-} effectively for complete precipitation. Therefore, a selective leaching system is needed for the synergistic treatment of spent LFP and NCM batteries.

To achieve such selectivity, we proposed in this study a salt leaching method to recycle valuable metals from spent LFP and $LiNi_{0.6}Co_{0.2}Mn_{0.2}O_2$ (NCM622) battery cathodes. The electrochemical measurements of electric potentials were conducted to evaluate redox ability. Based on this electrochemical study, the freely soluble ammonium ferric sulfate ($NH_4Fe(SO_4)_2$) was taken as an intermediate leaching agent for metal extraction from both cathodes. It was revealed that the introduction of ferric ions into this synergistic treatment can effectively extract valuable metals and completely precipitate phosphorus as ferric phosphate. The amount of ferric salt needed for the process was close to theoretical calculations (stoichiometric amount), and there were no other impurities released throughout the process. A thermodynamic study on the leaching solution is shown to be suitable for designing product recovery. The selective salt leaching by Fe^{3+} is a feasible approach for the green and efficient recycling of spent LIBs.

2 Experimental

2.1 Electrochemical test of reaction potentials

The reactants in this study include solid powders and aqueous solutions. Each gram of solid powder was mixed with 0.1 g carbon black, 0.25 g ethyl cellulose, 19 ml ethanol and 1.5 ml terpineol. The mixture was put in a beaker and stirred for 12 h, and then kept still for another 12 h. The supernatant of the mixture was spin-coated on a conductive glass, followed by a thermal treatment at 200 °C for 2 hours. The aqueous solution was prepared by mixing the tested salt with sodium sulfate (Na_2SO_4) in water. The concentration of each tested reactant was set at 0.1 M, with the Na_2SO_4 at 0.5 M to improve the electro-conductivity.

The electrochemical test was conducted with an electrochemical work station (produced by Corretest, Wuhan, China). Coated conductive glass was used as the working electrode and a platinum foil electrode as the auxiliary electrode. A Hg(s)|Hg_2SO_4(aq.)| and Sat. K_2SO_4(aq.) electrode (reference potential: 0.64 V *vs.* NHE) was used as the reference electrode. The electric potential was obtained by measuring the open circuit potential of each system and then calculated according to eqn (1):

$$E = E_m + E_{re} \quad (1)$$

where E is the system's actual electric potential, E_m is the measured potential, and E_{re} is the reference potential. The test was conducted when the system potential became stable, and each test lasted for 200 s.

2.2 Process for metal leaching and recovery

The flow process for leaching and recovery of metals from spent cathode materials is given in Scheme 1. Spent NCM and LFP cathode powders were mixed with the selected salt in a glass flask. Water was added at a solid to liquid ratio of 50 g L^{-1}. The leaching reaction was conducted in a water bath under different conditions. After the reaction, the solution and residue were separated in a centrifuge tube. In one treatment, the leaching residue was put into an $H_3PO_4/NH_4H_2PO_4$ buffer solution to regenerate $FePO_4{\cdot}2H_2O$. The pH was adjusted according to theoretical calculations using Visual Minteq software. After the reaction, the solid was heated at 600 °C under an air atmosphere for 1 h to burn carbon and other impurities.

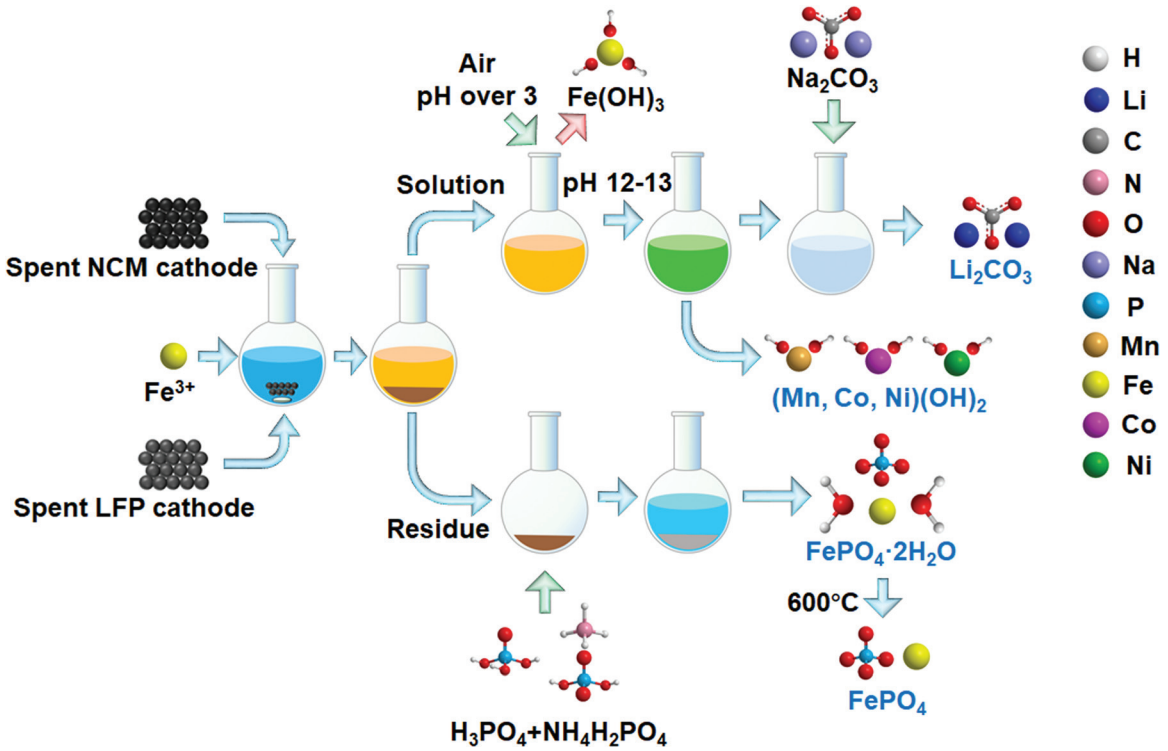

Scheme 1 Flow process for recycling of valuable components in NCM and LFP with Fe^{3+} as an intermediate.

In the other treatment, the solution was adjusted to a pH of over 3 and pumped with air to fully oxidize and precipitate the remaining Fe^{3+}/Fe^{2+}; it was then filtered with a 0.22 μm pore size filter. After filtration, NaOH was added to adjust the pH for Mn, Co and Ni precipitation. The precipitation pH was also designed based on thermodynamic calculations. The precipitates were separated and heated at 900 °C under an air atmosphere for 1 h to obtain metal oxides, while Na_2CO_3 was added into the supernatant to collect Li_2CO_3. The remaining alkaline solution can be used in gas control technology to absorb some acidic greenhouse or hazardous gases, including CO_2, SO_x and HCl to reduce their negative environmental impact.

2.3 Metal leaching efficiency analysis

To determine the composition of the spent NCM622 and LFP cathodes, the cathode powder was digested with aqua regia (composed of hydrochloric acid and nitric acid with a volume ratio of 3 : 1) using digestion apparatus, and then diluted with deionized water. The metal concentrations in the leachate were analyzed by inductively coupled plasma mass spectrometry (ICP-MS) using an Agilent Technologies 7700X ICP-MS. The leaching efficiency was calculated using eqn (2):

$$x = \frac{cV}{m} \quad (2)$$

where x is the leaching efficiency, c is the concentration of different metal ions in the leachate, V is the volume of leaching solution, and m is the initial mass content of the element in the cathode powder. The reaction mechanisms and activation energy were also determined based on leaching efficiencies measured at different times and temperatures. Different models including mass transfer in the liquid boundary layer, chemical reaction on the surface and diffusion in the solid surface layer were used to fit the experimental results.

2.4 Characterization of materials and products

Materials and products at different stages were ground into a powder and loaded on a silicon wafer and then characterized by X-ray diffraction (XRD) using a Rigaku Smartlab XRD operating at 45 kV and 200 mA. The scanning angle 2θ varied from 10 to 80° at a scanning rate of 5° per minute.

The morphology and element distribution of products were analyzed using a scanning electron microscope (SEM) equipped with an energy-dispersive X-ray spectrometer (EDX) and a Zeiss Merlin SEM. The scanning voltage for SEM and EDX mapping was set at 15 kV.

Elements and their valences in the products were analyzed by X-ray photoelectron spectroscopy (XPS) using a PHI 5000 Versaprobe III XPS. MultiPak software was used to assist in the identification of elements and their valences. The carbon binding energy was set at 284.8 eV for standard calibration.

3 Results and discussion

3.1 Design of the leaching system by reaction potentials

The synergistic reaction involves two parts, including reducing high valence Mn, Co and Ni into corresponding Mn^{2+}, Co^{2+}

and Ni^{2+},[30,40] and oxidizing $LiFePO_4$ into $FePO_4$.[41,42] NCM622 contains multiple transition metals with different valences. To understand the reduction reaction in the NCM622 cathode, the XPS analysis of its transition metals is given in Fig. 1a–c.

The main peak at 642.18 eV is assigned to Mn(IV), and the small peak at 636.89 eV is an Auger peak of Mn.[43–45] As for Co, the main peak at 779.71 eV and the weaker peak at 781.7 eV are assigned to Co(III) and Co(IV), respectively. The Ni in the cathode mainly exists as Ni(II) (854.53 eV) and Ni(III) (856.30 eV).[44–48] The satellite peak at 860.99eV is also assigned to Ni(II).[43,48] XPS peaks for Mn(III) in NCM111 or NCM523 are not detected.[47–49] Based on the results from XPS analysis, transition metals in $LiNi_{0.6}Co_{0.2}Mn_{0.2}O_2$ can be expressed as NiO, $NiO_{1.5}$, $CoO_{1.5}$, CoO_2, and MnO_2. The reduction reaction involving electron transfer in $LiNi_{0.6}Co_{0.2}Mn_{0.2}O_2$ expressed in eqn (3) can also be separated and written as eqn (4) (MO_x represents NiO, $NiO_{1.5}$, $CoO_{1.5}$, CoO_2, and MnO_2).

$$LiNi_{0.6}Co_{0.2}Mn_{0.2}O_2 + 4H^+ + e^- = Li^+ + 0.6Ni^{2+} + 0.2Co^{2+} + 0.2Mn^{2+} + 2H_2O \quad (3)$$

$$MO_x + 2xH^+ + (2x-2)e^- = M^{2+} + xH_2O \quad (4)$$

The measured reaction potentials of transition metal reductions in $LiNi_{0.6}Co_{0.2}Mn_{0.2}O_2$ are given in Fig. 1d and

Table 1 Reaction potentials of related redox couples and their corresponding pH

Redox couple	E (V)	pH
$LiNi_{0.6}Co_{0.2}Mn_{0.2}O_2/Ni^{2+}$	0.6419	7.08
$LiNi_{0.6}Co_{0.2}Mn_{0.2}O_2/Co^{2+}$	0.5833	7.22
$LiNi_{0.6}Co_{0.2}Mn_{0.2}O_2/Mn^{2+}$	0.4094	7.17
$FePO_4/LiFePO_4$	0.1841	8.10
Fe^{3+}/Fe^{2+}	0.6077	2.30
$Fe(OH)_3/Fe^{2+}$	0.4890	3.36

Table 1. The oxidation potential of $LiFePO_4$ into $FePO_4$ (eqn (5)) was also determined.

$$FePO_4 + Li^+ + e^- = LiFePO_4 \quad (5)$$

It is noticed that the reaction conditions of the electrochemical test (pH and ion concentrations) were not the same as the metal leaching conditions. Therefore, the potentials are converted into the actual pH and concentration by the Nernst equation as given in eqn (6).

$$a\ \mathrm{ox} + ne^- \rightarrow b\ \mathrm{red}$$

$$E(\mathrm{ox/red}) = E^{\theta}(\mathrm{ox/red}) + \frac{0.0591}{n}\lg\frac{[c(\mathrm{ox}/c^{\theta})]^a}{[c(\mathrm{red}/c^{\theta})]^b} \quad (6)$$

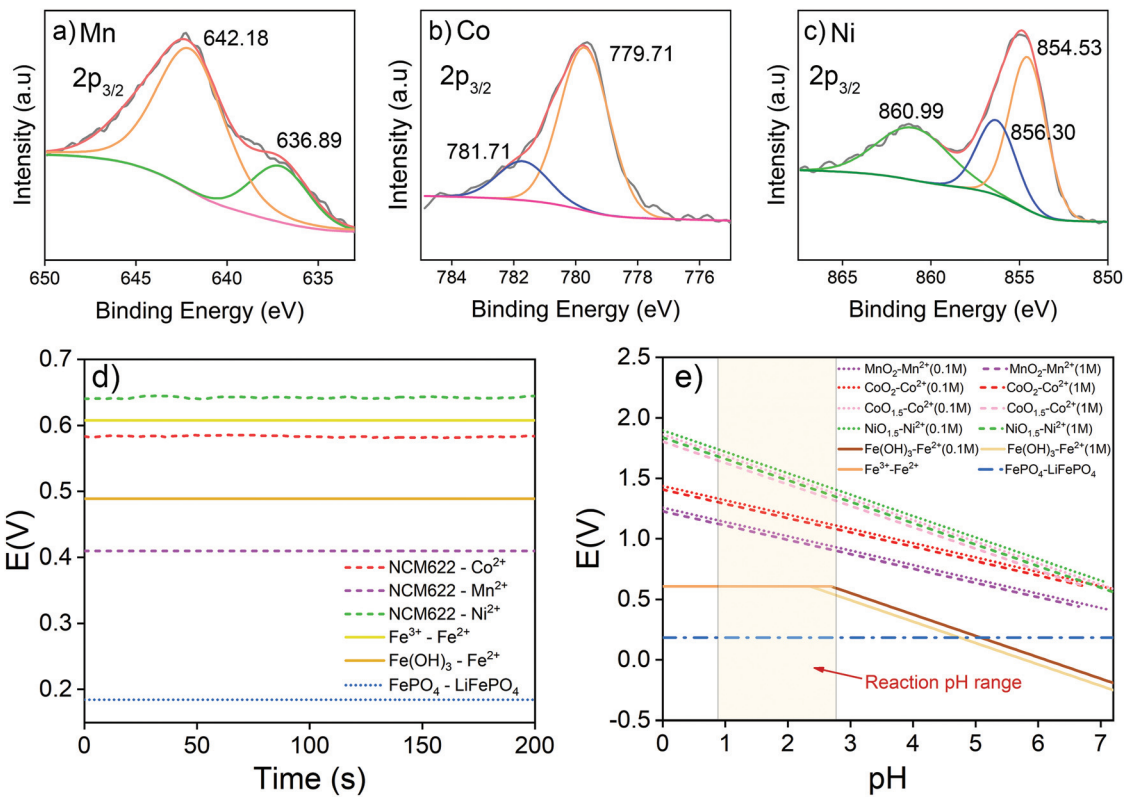

Fig. 1 XPS spectra of (a) Mn, (b) Co, and (c) Ni from the spent NCM622 cathode material; (d) reaction potentials of redox couples; and (e) calculated reaction potentials of redox couples at different pH values according to the Nernst equation.

In this study, reactions on NCM622 involved the participation of H^+; therefore, the redox reaction is affected by the acidity of the system. The Nernst equation is expressed as eqn (7) (MO_x = NiO, $NiO_{1.5}$, $CoO_{1.5}$, CoO_2, and MnO_2):

$$E(MO_x/M^{2+}) = E^{\theta}(MO_x/M^{2+}) + \frac{0.0591}{2x-2}\lg\frac{[H^+]^{2x}}{[M^{2+}]} \quad (7)$$

The oxidation of $LiFePO_4$ into $FePO_4$ does not involve the acidity or the concentration of the redox couple. Therefore, the potential remains unchanged under the test conditions. The variation of calculated reaction potentials with pH and the concentration of redox couples is given in Fig. 1e. In this study, the solid-to-liquid ratio (S/L) was set at 50 g L^{-1}. Concentrations of metal elements in the solution ranged from 0.1 to 1 M. However, as revealed in Fig. 1e, the concentration differences do not have as much influence as pH on redox reaction potentials. The acidity of the solution is the dominant factor for the redox reactions of NCM and LFP, and a lower pH is preferable. NCM622 and LFP are both insoluble solids, and a water-soluble intermediate is needed for effective reaction. To avoid introducing more elements into the system, the Fe^{3+} was assumed to be a good candidate of intermediates.

The ionic Fe^{3+} can only exist at low pH, whereas at pH higher than 3, it will be transferred into $Fe(OH)_3$ precipitates. Redox potentials for an Fe^{3+}/Fe^{2+} couple and an $Fe(OH)_3/Fe^{2+}$ couple are given in Fig. 1d and Table 1. The redox reactions are represented by eqn (8) and (9), with their corresponding redox reaction potentials at different concentrations and pH being calculated (eqn (10) and (11)) and shown in Fig. 1e.

$$Fe^{3+} + e^- = Fe^{2+} \quad (8)$$

$$Fe(OH)_3 + 3H^+ + e^- = Fe^{2+} + 3H_2O \quad (9)$$

$$E(Fe^{3+}/Fe^{2+}) = E^{\theta}(Fe^{3+}/Fe^{2+}) + \frac{0.0591}{1}\lg\frac{[Fe^{3+}]}{[Fe^{2+}]} \quad (10)$$

$$E(Fe(OH)_3/Fe^{2+}) = E^{\theta}(Fe(OH)_3/Fe^{2+}) + \frac{0.0591}{1}\lg\frac{[H^+]^3}{[Fe^{2+}]} \quad (11)$$

When Fe(III) exists as ionic Fe^{3+}, the electric potential remains unchanged with pH, but when Fe(III) exists as Fe $(OH)_3$, the potential decreases with increasing pH. On the one hand, the electric potential of Fe(III)/Fe^{2+} is always lower than those of Mn, Co, and Ni from NCM622, which indicates that NCM622 can be reduced by Fe^{2+}. On the other hand, it is predictable that at pH values higher than 5, $Fe(OH)_3$ will no longer be able to oxidize $LiFePO_4$ into $FePO_4$. According to these analyses, Fe^{3+} should be an effective intermediate for the synergistic treatment of NCM and LFP at low pH. Since Fe^{3+} can already provide an acidic environment, additional acid should not be needed for the metal extraction reaction. In conclusion, an electrochemical study is shown to be a convenient approach to design redox additives.

3.2 Analysis of the leaching process

The NCM and LFP cathodes are both insoluble solid powders. Therefore, a water-soluble Fe(III) salt is needed to act as an intermediate for an effective reaction. $FeCl_3$ and $Fe(NO_3)_3$ were not suitable here because they have potential to generate hazardous Cl_2 or NO_x.[16] Therefore, ferric sulfate including $Fe_2(SO_4)_3$ and $NH_4Fe(SO_4)_2$ (which existed as $NH_4Fe(SO_4)_2{\cdot}12H_2O$) were selected for the metal leaching test. The comparison of the leaching effect between $Fe_2(SO_4)_3$ and $NH_4Fe(SO_4)_2$ is given in Fig. S1.† The results reveal a better leaching performance of $NH_4Fe(SO_4)_2$ than that of $Fe_2(SO_4)_3$. The superior performance of $NH_4Fe(SO_4)_2{\cdot}12H_2O$ is attributed to its higher dissolution rate and hence more Fe^{3+} released into the solution in a shorter time. In contrast, the dissolution of $Fe_2(SO_4)_3$ into water is a slow process, and thus the whole reaction rate is limited. The limit of slow dissolution of $Fe_2(SO_4)_3$ was confirmed by conducting an additional test by using $Fe_2(SO_4)_3$ solutions as the intermediate in the leaching test. The results in Fig. S2† show a significantly improved leaching efficiency by using $Fe_2(SO_4)_3$ aqueous solutions as compared with the addition of $Fe_2(SO_4)_3$ powders. In fact, leaching using $Fe_2(SO_4)_3$ aqueous solutions could achieve similar (Li and Mn) or better (Co and Ni) efficiencies as compared with the case of using $NH_4Fe(SO_4)_2{\cdot}12H_2O$ in the powder as the intermediate. This finding suggests a great benefit of using aqueous solutions rather than powder forms of the intermediates, which will be further tested as an important parameter in the upcoming scale up tests and reported in a separate communication. Furthermore, an overdose of $Fe_2(SO_4)_3$ to fully extract the transition metals from NCM622 inevitably leads to some extra Fe^{2+} in the liquid that needs to be oxidized after leaching. Higher pH is desirable for oxidation and removal of Fe^{2+} (Fig. 1e) but it may also lead to the precipitation of other transition metals. The ammonium present can form a complex with Mn, Co and Ni, preventing them from precipitating at an early stage and providing more flexibility for treating the remaining Fe^{2+}. Therefore, $NH_4Fe(SO_4)_2{\cdot}12H_2O$ was selected as a leaching intermediate in this study.

3.2.1 Optimization of leaching conditions. The optimized leaching conditions were determined by varying different leaching parameters. The internal variate included the mass ratio between LFP and NCM622, and the amount of $NH_4Fe(SO_4)_2{\cdot}12H_2O$. The external variate included the reaction temperature and time.

The influence of the mass ratio between LFP and NCM622 is given in Fig. 2a and Fig. S3.† LFP and NCM622 theoretically react at a molar ratio of 1 : 1. The mass ratio is therefore calculated to be LFP/NCM622 = 1.63. Leaching results show that LFP/NCM622 > 1.8 is suitable for high-efficiency metal extraction where over 97% valuable metals can be extracted from both cathodes. For a higher mass ratio, the leaching efficiency of Li, Mn, Co, and Ni does not change markedly, but excessive Fe^{2+} will be generated, which needs additional oxidation by air or another oxidant to separate it from other transition metals. Therefore, LFP/NCM622 = 1.8 is a suitable composition.

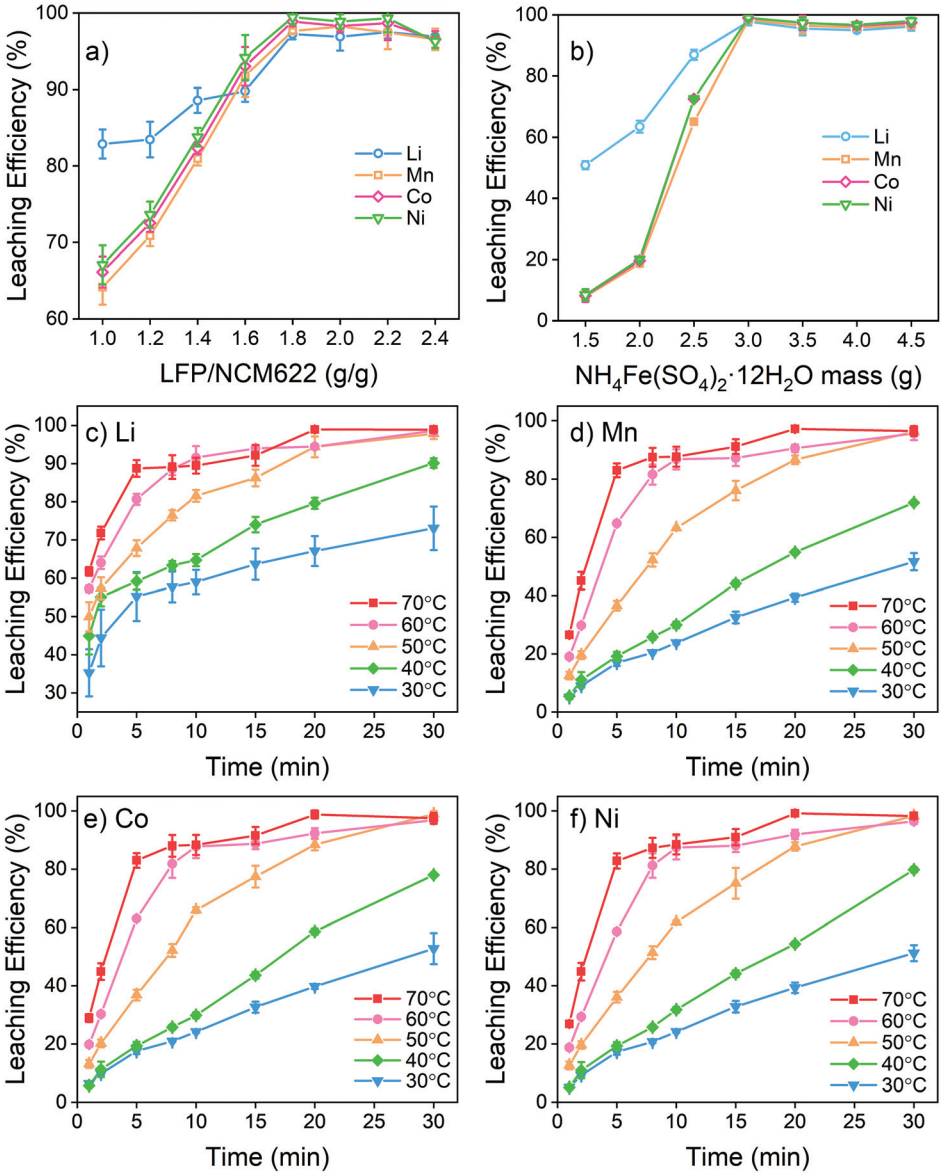

Fig. 2 (a) Leaching efficiency of metals at different LFP/NCM622 mass ratios (g g^{-1}) with $NH_4Fe(SO_4)_2{\cdot}12H_2O$/mixed cathode powder = 3 : 1 (g g^{-1}) at 50 °C for 30 min; (b) leaching efficiencies of metals with different amounts of $NH_4Fe(SO_4)_2{\cdot}12H_2O$ with LFP/NCM622 = 1.8 (g g^{-1}) at 50 °C for 30 min; and (c–f) leaching efficiencies of metals at different temperatures and times with LFP/NCM622 = 1.8 (g g^{-1}) and $NH_4Fe(SO_4)_2{\cdot}12H_2O$/mixed cathode powder = 3 : 1 (g g^{-1}).

The amount of $NH_4Fe(SO_4)_2{\cdot}12H_2O$ added is also important for full metal extraction. According to the reaction function, it is theoretically predicted that 2.56 g of $NH_4Fe(SO_4)_2{\cdot}12H_2O$ is needed for complete metal extraction from 1 g of the mixed powders. It is revealed in Fig. 2b that at least 3 g of $NH_4Fe(SO_4)_2{\cdot}12H_2O$ is needed to fully extract the metals. Excessive Fe^{3+} introduced into the solution does not have any more positive influence on leaching efficiency or other process behaviors. Therefore, 3 g of $NH_4Fe(SO_4)_2{\cdot}12H_2O$ to treat 1 g of mixed powder (LFP/NCM622 = 1.8) is proposed to be the optimized internal condition. Under the optimized internal conditions, the system pH is found to be 0.91 at the beginning and 2.88 after the reaction is completed (as colored in Fig. 1e). According to the electrochemical study discussed earlier, such a pH range is assumed to be suitable for the redox reaction between $LiNi_{0.6}Co_{0.2}Mn_{0.2}O_2$ and $LiFePO_4$ with the assistance of the intermediate Fe^{3+}. The leaching efficiency of phosphate is given in Fig. S4 and S5.† PO_4^{3-} is not extracted in all tests, which is different from the leaching with a strong inorganic acid. With the addition of Fe^{3+} into the system, the phosphate remains as residue. Previous studies also showed that PO_4^{3-} remains as a $FePO_4$ solid in such a pH range.[50,51] The high-efficiency selective leaching demonstrates that the proposed electrochemical test and calculation method are applicable for treating mixed spent LIB cathodes with different redox properties.

The external reaction conditions including temperature and time were also investigated, and the results are given in Fig. 2c–f. Higher temperatures and longer reaction times were shown to improve the leaching efficiencies. With increasing temperatures, the leaching time for full extraction is reduced gradually. According to the experimental results, 50 °C and 30 min are regarded as suitable conditions. During the leaching process, Li is extracted from both $LiNi_{0.6}Co_{0.2}Mn_{0.2}O_2$ and $LiFePO_4$, featuring a faster leaching rate than transition metals. At 30 °C, for example, over 50% of Li is already released into the solution within 5 min. Mn, Co and Ni are known to be uniformly distributed in the cathode structure. Therefore, even though they have different redox potentials, they eventually have similar leaching characteristics and are simultaneously released into the solution.

In summary, the optimal leaching conditions are determined to be LFP/NCM622 = 1.8 (g g^{-1}) and $LiNi_{0.6}Co_{0.2}Mn_{0.2}O_2$/mixing cathode = 3 (g g^{-1}) at 50 °C and 30 min. Under these conditions, valuable metals from both LFP and NCM622 cathodes can be effectively extracted, while the Fe^{2+} and Fe^{3+} that need further treatment are minimized.

A comparison of cathode material leaching from NCM and LFP is given in Table 2. In most studies, inorganic acids or organic acids are used as leaching agents to extract metals from the cathode. Additional reductants for LCO and NCM, or oxidants for LFP, are also necessary to improve the leaching efficiency. Compared with the results from previous studies, the leaching process developed in this study does not require the addition of an acid. Moreover, the intrinsic redox reaction between $LiNi_{0.6}Co_{0.2}Mn_{0.2}O_2$ and $LiFePO_4$ also reduces the additional reductant or oxidant to a large extent. Synergistic leaching is a feasible method for treating mixed cathodes from spent LIBs.

3.2.2 Reaction kinetics and mechanism. In order to clearly understand the reaction mechanism, a comparison of results using $NH_4Fe(SO_4)_2$ to leach LFP and NCM622 individually or synergistically is given in Fig. S6.† It can be noticed that $NH_4Fe(SO_4)_2$ is able to fully react with LFP and release Li^+, while it has limited leachability for NCM. With the addition of LFP, metals from NCM were able to be reduced and leached out. With the addition of 1,10-phenanthroline in the $NH_4Fe(SO_4)_2$ – LFP group, the red color of the liquid reveals the generation of Fe^{2+} (Fig. S7†). The whole reaction process can therefore be divided into two steps of solid–liquid reactions. In the first step, the Fe^{3+} added is reduced by $LiFePO_4$ to produce Fe^{2+} as expressed in eqn (8). In the second step, the Fe^{2+} produced reduced $LiNi_{0.6}Co_{0.2}Mn_{0.2}O_2$ to Mn^{2+}, Co^{2+} and Ni^{2+} (eqn (12)). The H^+ came from the hydrolyzation of Fe^{3+} as expressed in eqn (13). With the consumption of H^+ in the second step, more $Fe(OH)_3$ was generated. The overall reaction between LFP and NCM622 with Fe^{3+} as an intermediate can be expressed as eqn (14).

$$LiNi_{0.6}Co_{0.2}Mn_{0.2}O_2 + Fe^{2+} + 4H^+ = Li^+ + 0.6Ni^{2+} + 0.2Co^{2+} + 0.2Mn^{2+} + Fe^{3+} + 2H_2O \quad (12)$$

$$Fe^{3+} + 3H_2O \leftrightarrow Fe(OH)_3 + 3H^+ \quad (13)$$

$$LiNi_{0.6}Co_{0.2}Mn_{0.2}O_2 + LiFePO_4 + \frac{4}{3}Fe^{3+} + 2H_2O = 2Li^+ + 0.6Ni^{2+} + 0.2Co^{2+} + 0.2Mn^{2+} + FePO_4 + \frac{4}{3}Fe(OH)_3 \quad (14)$$

The reaction kinetics was studied in terms of various solid–liquid reaction models. In general, the solid–liquid reaction is controlled by the following three factors: mass transfer in the liquid boundary layer (eqn (15)), chemical reaction on the surface (eqn (16)) and diffusion in the solid surface layer (eqn (17)).[53,55]

$$x = k_1 t \quad (15)$$

$$1 - (1 - x)^{1/3} = k_2 t \quad (16)$$

$$1 - 3(1 - x)^{2/3} + 2(1 - x) = k_3 t \quad (17)$$

where x refers to leaching efficiency during the reaction time t (min), and k_1, k_2 *and* k_3 are the reaction rate constants (min^{-1}). The activation energy of the leaching process is calculated based on the Arrhenius equation described in eqn (18):

$$\ln k = -\left(\frac{E_a}{R}\right)\frac{1}{T} + \ln A \quad (18)$$

where k represents the reaction rate constant (min^{-1}), A is the pre-exponential factor, T represents the temperature of the reaction (K), E_a is the activation energy of the reaction (J mol^{-1}), and R is the universal gas constant (8.314 J mol^{-1} K^{-1}).

Table 2 Leaching results of metals from cathodes by different leaching agents

Cathode	Leaching agent	Conditions	Efficiency	Ref.
NCM, LFP	0.3 M $NH_4Fe(SO_4)_2$	50 g L^{-1}, 50 °C, 30 min	97.8% Li, 98.3% Mn, 98.9% Co, 99.0% Ni	This study
NCM, LFP	0.25 M H_2SO_4	32 g L^{-1}, 80 °C, 4 h	>96% Li, Mn, Co, Ni	38
LCO, LFP	0.5 M H_2SO_4	30 g L^{-1}, 20 min	99% Li, Fe, P, 92.4% Co	39
LCO, LMO, NCM, LFP	4 M H_2SO_4, 30% H_2O_2	70–80 °C, 2–3 h	Li, Mn, Co, Ni dissolved, LFP partly dissolved	51
LCO	2 M H_2SO_4, 6% H_2O_2	100 g L^{-1}, 60 °C, 1 h	97% Li, 98% Co	19
LCO	1.25 M citric acid, 1% H_2O_2	20 g L^{-1}, 90 °C, 30 min	100% Li, >90%Co	21
NCM	2.5 M H_2SO_4, 0.8 M NH_4Cl	100 g L^{-1}, 80 °C, 1 h	99.11% Li, 97.34% Mn, 97.55% Co, 97.49% Ni	52
NCM	3 M formic acid, 6% H_2O_2	50 g L^{-1}, 60 °C, 2 h	98.22% Li, 99.95% Mn, 99.96% Co, 99.96% Ni	53
LFP	0.3 M H_2SO_4, H_2O_2/Li = 2.07, H_2SO_4/Li = 0.57	60 °C, 2 h	96.85% Li	29
LFP	0.8 M acetic acid, 6% H_2O_2	120 g L^{-1}, 50 °C, 30 min	95.05% Li	54

The fitting of the data to these leaching reaction models and the corresponding fitting parameters are given in Fig. 3a–d, while others are given in Fig. S8 and S9.†

According to the fitting results, the leaching of transition metals Mn, Co and Ni is mainly controlled by the surface chemical reactions. At a relatively low leaching temperature of 30 °C and 40 °C, the reaction is also influenced by mass transfer. Lower leaching temperatures led to slow precipitation of $FePO_4$ and $Fe(OH)_3$ with the precipitates being dispersed in solution to increase the viscosity of the system. The increasing leaching temperature increases the thermal energy and hence weakens interactions among the molecules in solution, which decreases the system viscosity. At the same time, increasing the leaching temperature also increases the rate of $FePO_4$ and $Fe(OH)_3$ precipitation. Under these conditions, the influence of mass transfer becomes weaker. In this study, it was found that surface diffusion does not have a noticeable impact on transition metal leaching. Finally, the fitting of activation energy given in Fig. S10† shows an increase in apparent activation energies of 47.47, 53.21, 55.39 and 58.03 kJ mol^{-1} for Li, Ni, Co and Mn, respectively.

The leaching rate of Li is higher than those of transition metals and kinetic analysis reveals that the reaction of Li is influenced by both surface chemical reaction and diffusion. However, at 30 °C, the leaching result of Li does not fit well with any of the models. In the first minute, a large amount (more than 30%) of Li was leached out rapidly into the solution. After 2 minutes of leaching, Li exhibited a similar leaching trend to other transition metals. The analysis of the reaction mechanisms is given in Fig. 3e. Li comes from both $LiFePO_4$ and $LiNi_{0.6}Co_{0.2}Mn_{0.2}O_2$. $LiFePO_4$ has an olivine crystal structure and Li stays in octahedral voids. With a small ion radius, Li^+ is easy to transfer without changing the structure of $LiFePO_4$.

Similar to the working mechanism of LFP, the oxidation of $LiFePO_4$ by Fe^{3+} simply involves the electron transfer and release of Li^+, while the whole olivine structure of $LiFePO_4$ is not destroyed during the reaction.[54,56] The reaction is simple and can proceed at a fast rate, which explains the high leaching efficiency of Li in the first few minutes. The redox reaction between Fe^{2+} and $LiNi_{0.6}Co_{0.2}Mn_{0.2}O_2$ on the other hand is more complicated. The LCO and NCM cathodes have layered structures formed by Mn, Co, Ni and oxygen. Li exists as interlaid ions in the voids between the layers. During the redox reaction, electron transfer occurs between Fe^{2+} from the solution and Mn, Co and Ni from the cathode. The H^+ generated by Fe^{3+} hydrolysis needs to break chemical bonds in the layer structure to take away the oxygen. Mn, Co and Ni can only be released after the structure is destroyed.[57,58] Therefore, compared with the oxidation of $LiFePO_4$, the reduction of $LiNi_{0.6}Co_{0.2}Mn_{0.2}O_2$ has a slower reaction rate and becomes the controlling process of the whole reaction.

3.3 Product recovery and analysis

The degradation of LIBs is usually caused by a number of processes, including structural failure, aging and decomposition of components, and overgrowth of the solid electrolyte interphase.[13,59,60] Most of the metals are preserved in the battery cell. The recovered metals are proposed to generate new materials after separation and proper treatment. In this study, the leaching system includes components from both LFPs and NCMs. The study aimed at separating various components into the Fe–P system and Ni–Co–Mn system as in the form of original batteries. In the current case, the precursors $FePO_4$, NiCoMn oxides and Li_2CO_3 were proposed to be synthesized. To obtain pure products, thermodynamic calculations on solution systems were conducted to assist in determining the experimental conditions.

3.3.1 Recovery and characterization of $FePO_4$. The residue obtained after leaching is mainly composed of $FePO_4$ and $Fe(OH)_3$. The excessive amount of Fe(III) from $Fe(OH)_3$ needs to be balanced by additional phosphorus to obtain $FePO_4$. Fe^{3+} is known as a ternary weak base that can hydrolyze to become different hydroxides and ions. H_3PO_4 is a ternary moderate acid that can exist in multiple forms with different numbers of H^+ being deprotonized. The acidity of the system is expected to be the dominant factor for ion concentrations and solid-phase species. To determine proper conditions, thermodynamic calculations on related species were systematically conducted using Visual Minteq software as described in the Experimental section, and the results are given in Fig. 4a.

Extra water-soluble H_3PO_4 and $NH_4H_2PO_4$ were added to adjust pH and to balance Fe. Species with concentrations below 10^{-6} M in the calculated range were considered negligible in the solution. At pH below 1, there are still considerable amounts of different Fe(III) ion species including Fe^{3+} and $FeH_2PO_4^{2+}$ in solution. The solid phase is simply $FePO_4$, in equilibrium with the corresponding soluble species. At low pH, the ionization of H^+ from H_3PO_4 is known to be impeded, which limits the combination of Fe^{3+} and PO_4^{3-}. All Fe(III) ion species decrease in concentration with increasing pH. Fe(III) is predicted to be completely precipitated out at pH above 2. However, when the pH exceeds 4.5, the $FePO_4$ precipitates are converted into $Fe(OH)_3$. Therefore, in this study, the leaching residue was washed with an H_3PO_4–$NH_4H_2PO_4$ solution at pH 2–3. The product after washing is verified to be ferric phosphate hydrate ($FePO_4{\cdot}2H_2O$) with two kinds of crystal structures (Fig. S11†). To clarify the component and eliminate the possible impurities, the product was calcined under an air atmosphere at 600 °C. As given in Fig. 4b, the anhydrous $FePO_4$ is obtained after the calcination. The SEM image and EDX mapping in Fig. 4c–e show that P and Fe distribute uniformly in the product. Other metal elements (Ni, Co or Mn) from NCM cathodes are not detected in the recovered $FePO_4$. The results suggest that such a method is feasible for $FePO_4$ recovery and the product can be used to produce a second LFP cathode material.

3.3.2 Recovery and characterization of NiCoMn oxides. The transition metals Mn, Co, and Ni are leached into the solution and the precipitation is a good method for their recovery. In a alkaline environment, these transition metals are known to form precipitates completely.[50] As mentioned, the introduction

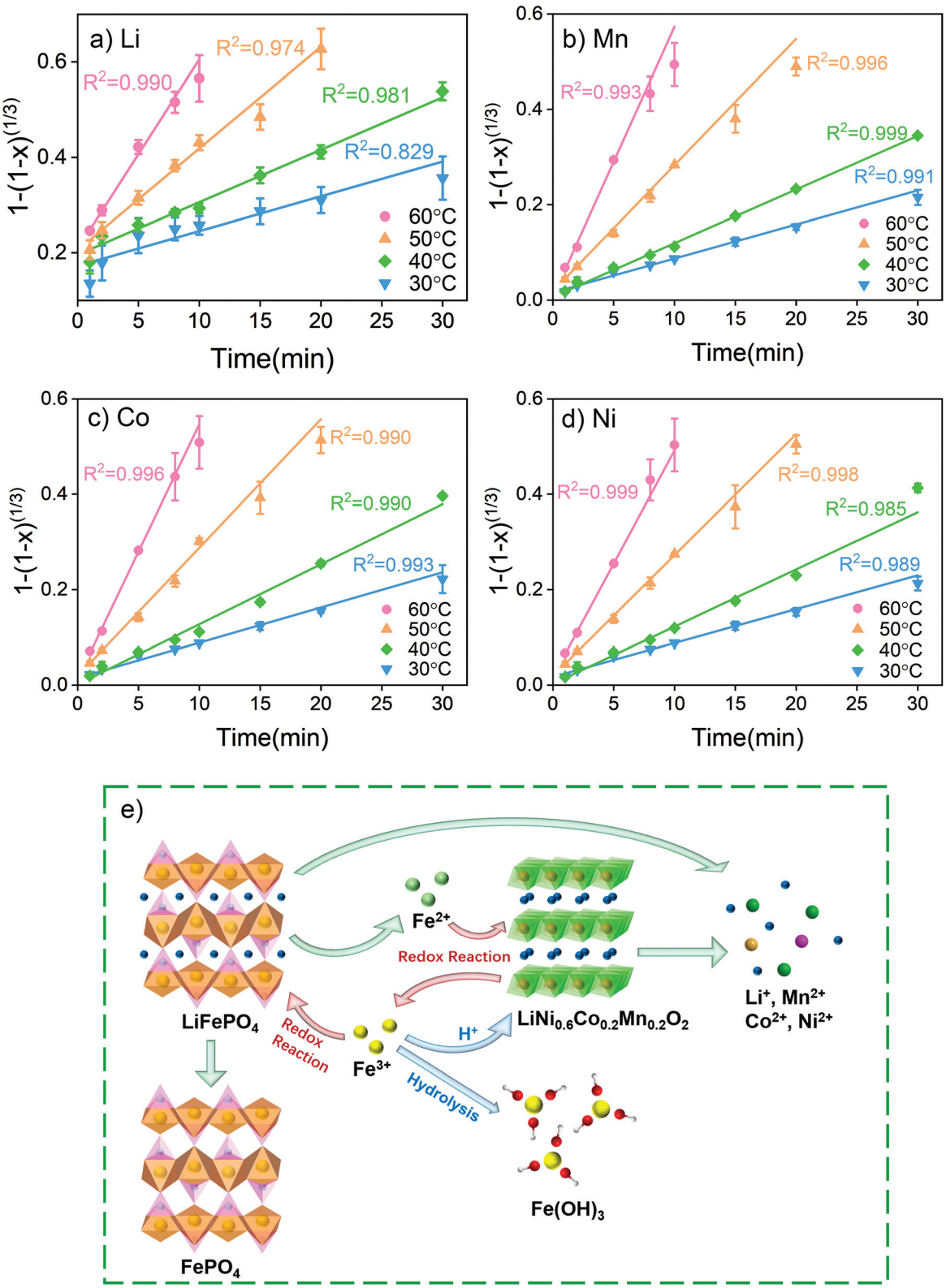

Fig. 3 (a) Fitting results of (a) Li, (b) Mn, (c) Co and (d) Ni, according to a surface chemical reaction model, and (e) reaction mechanisms of synergistic metal extraction from NCM and LFP using Fe^{3+} as an intermediate.

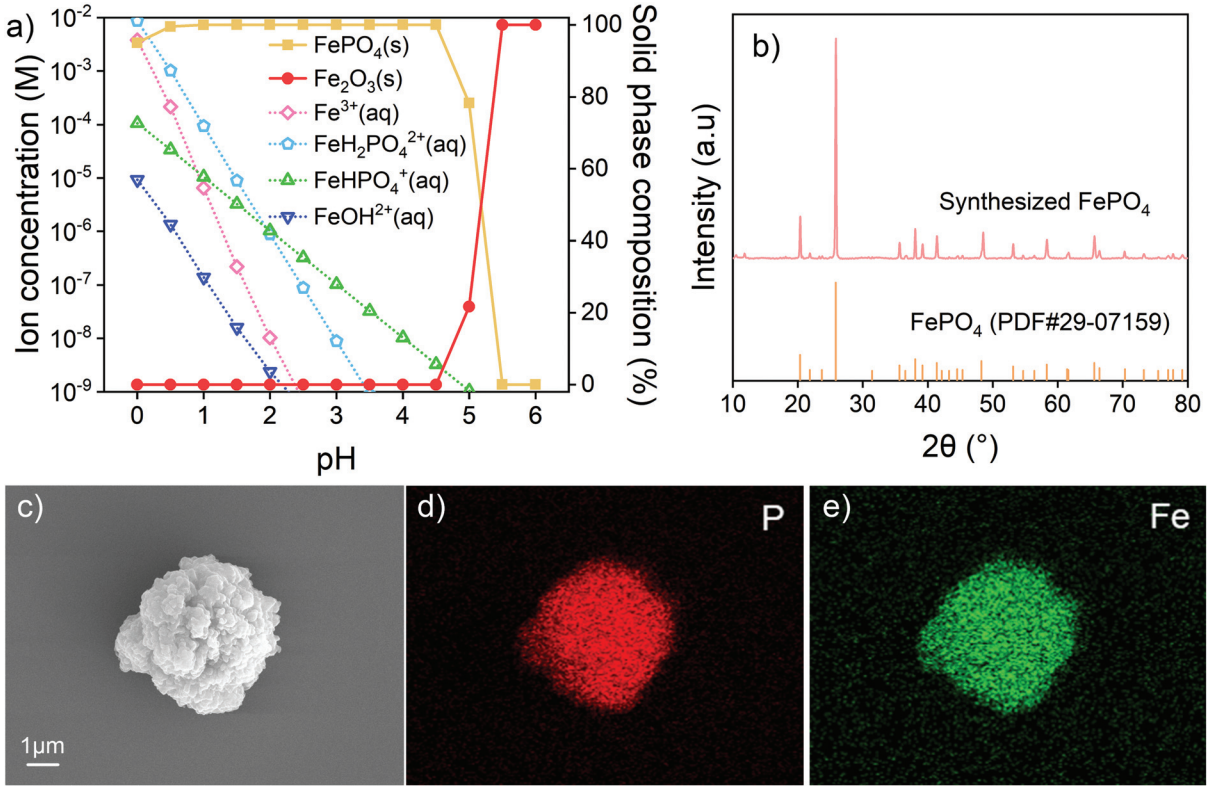

Fig. 4 (a) Calculated ion concentrations and solid phase compositions of Fe(III)-PO_4^{3-} at different pH values; (b) XRD pattern and (c) SEM image of synthesized $FePO_4$ after 600 °C calcination; EDX mapping images of (d) P and (e) Fe from synthesized $FePO_4$ after 600 °C calcination.

of NH_4^+ into the solution by $NH_4Fe(SO_4)_2$ may also lead to the formation of the ammonium complex in the alkaline environment. In some previous studies, ammonium leaching has also been applied as a metal leaching method.[61,62] Therefore, thermodynamic calculations were also performed to investigate suitable precipitating conditions and the results are given in Fig. 5a and b. According to Fig. 5a, the concentration of Mn^{2+}, Co^{2+}, and Ni^{2+} decreases with increasing pH. When the pH is lower than 10 (a weakly alkaline environment), some of the Mn, Co and Ni will combine with NH_3 to form soluble complexes $Mn(NH_3)_n^{2+}$, $Co(NH_3)_n^{2+}$, and $Ni(NH_3)_n^{2+}$. Based on the results of solution chemistry calculations, the concentration of $Ni(NH_3)_n^{2+}$ increases on increasing the pH to 9.5. Then its concentration decreases with further increase in the basicity of the solution. A similar trend is found for Mn, but the highest concentration is obtained around pH 8.5. As for Co, its ammonium complex concentration decreases gradually with increasing basicity of the solution. At pH > 12, all forms of the ammonium complex were precipitated or transferred into other kinds of ion complexes. Therefore, the precipitation pH should not be lower than 12.

Mn, Co and Ni can also combine with OH^- to form complex ions in a strongly alkaline environment. Concentrations of $Mn(OH)_n^{2-n}$, $Co(OH)_n^{2-n}$ and $Ni(OH)_n^{2-n}$ follow a similar trend where they first decrease and then increase with increasing pH. Fig. 5b also shows the influence of pH on the recovery of the transition metal precipitate. With increasing basicity, $Ni(OH)_2$ is first precipitated and fully recovered, followed by $Co(OH)_2$ and $Mn(OH)_2$. This finding indicates that the pH should be higher than 11.5 to fully precipitate the transition metals. To fully recover the transition metals as hydroxides, the system pH of 12–13 is considered suitable.

After filtration and separation, the remaining alkaline solution needs to be neutralized to reduce its potential negative impact on the environment. It can be used to absorb acidic greenhouse gases or industrial off gas including CO_2, SO_x and HCl which may bear implications of carbon neutralization or reduction in emissions of other toxicities into the environment. Normally, the acidic off gas from industrial production requires neutralization by an additional alkali (*e.g.*, CaO and NaOH). During such treatment with the remaining solution, ammonium and sodium salts can be obtained, with the water being reused in the process and air pollution reduced. The recovered transition metal hydroxides were dried and calcined at 900 °C for full decomposition to obtain metal oxides. Fig. 5c shows the solids of NiO and $MnCo_2O_4$ crystal structures after the calcination, indicating the presence of transition metals from the NCM cathode. The XPS analysis of the calcined metal oxides is given in Fig. S12.† The valences of transition metals in the recovered solids were found to be the same as that in the raw material, which provides the possibility of regeneration

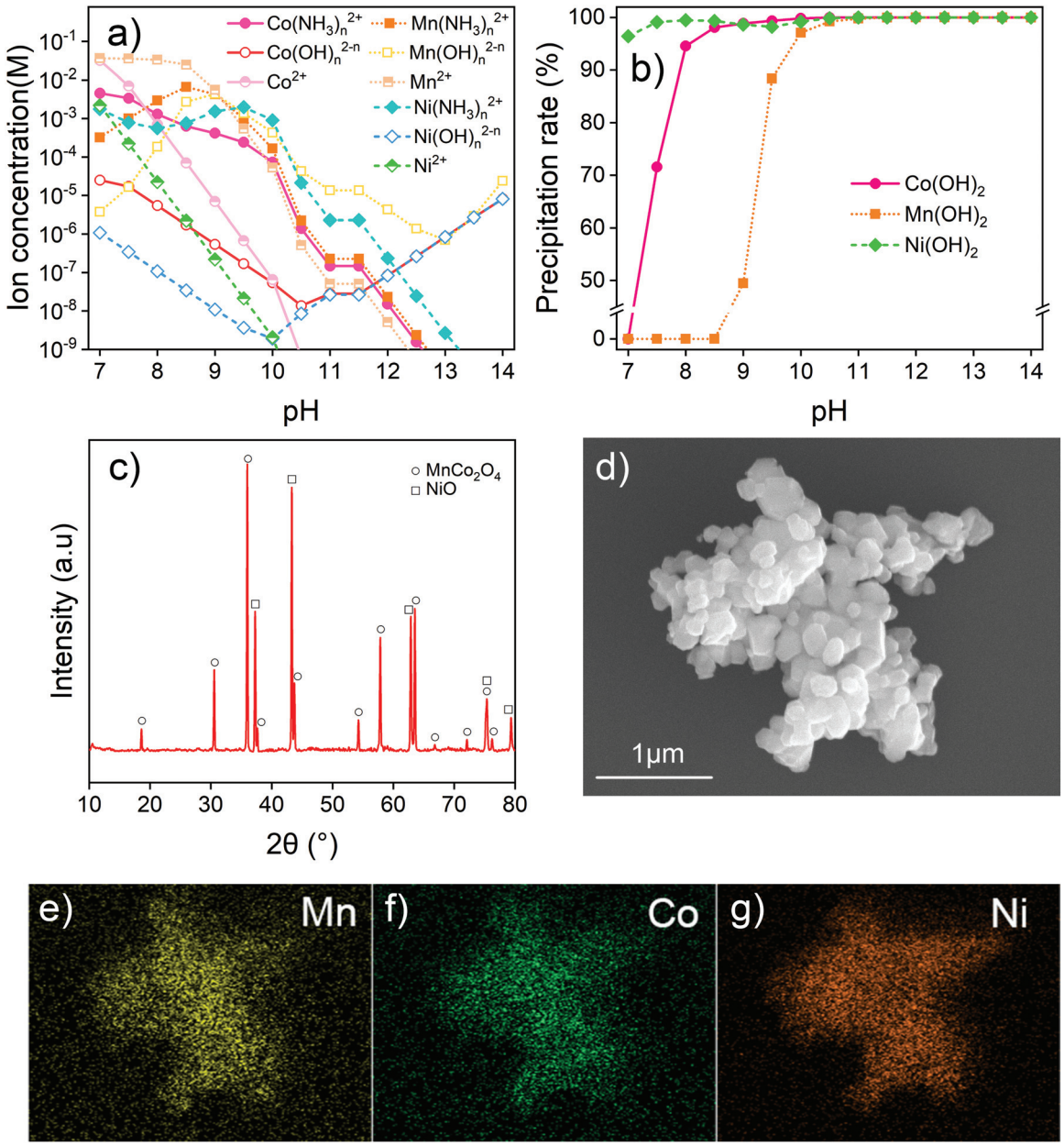

Fig. 5 (a) Calculated ion concentrations of Mn(II), Co(II), and Ni(II) at different pH values. (b) Precipitation rate of $Mn(OH)_2$, $Co(OH)_2$, and $Ni(OH)_2$ at different pH values. (c) XRD pattern and (d) SEM image of the synthesized MnCoNi oxide after 900 °C calcination. EDX mapping image of (e) Mn, (f) Co, and (g) Ni from the synthesized MnCoNi oxide after 900 °C calcination.

of new materials. The SEM and EDX mapping images of the calcined mixed oxides are given in Fig. 5d–g, showing the calcined products as fine particles with little agglomeration. Ni, Co and Mn have a nearly uniform distribution. Other elements, such as Fe or P from LFPs, are not detected. The analysis of the product indicates that not only is the selective leaching method by Fe^{3+} suitable for the effective recovery of transition metals from NCM, but also the recovered product can be used to regenerate new materials with proper precipitation and calcination.

In short, the salt leaching by Fe^{3+} selected from the electric potential measurements can achieve synergistic treatment of spent NCMs and LFPs. Li, Mn, Co and Ni can all be fully extracted while $FePO_4$ is completely separated and preserved in residues. Therefore, it is anticipated that this salt leaching method will be effective for treating mixed spent battery cathodes with high efficiency and selectivity. Moreover, the product recovery is designed based on thermodynamic calculations and the experimental results are consistent with the predictions. Therefore, it can be concluded that a theoretical study is

feasible for designing reaction conditions for a solution system and such a method is expected to have a wide applicability in designing metal solution reactions.

4 Conclusions

Reducing the consumption of acid and redox additives in hydrometallurgical recycling of valuable metals from spent LIBs is the desired objective. In this study, we proposed the application of an electrochemical method by measuring the electric potential to determine the proper intermediate salt for synergistically treating spent LFPs and NCMs. Based on the test results, Fe^{3+} was found to be a suitable intermediate, and the theoretical predictions were verified by the results of leaching experiments. The water-soluble $NH_4Fe(SO_4)_2$ was proven to be suitable as a leaching agent. By adjusting the leaching parameters, Li and transition metals from NCM cathodes can be effectively extracted under mild conditions, while Fe and PO_4^{3-} from LFPs remain in solid residues. The kinetic study indicates that the reaction rate is mainly controlled by a surface chemical reaction between Fe^{2+} and the NCM cathode, which is explained by the structure destruction of the NCM cathode. A systematic thermodynamic study on the solution was conducted to design the recovery strategy of metals, and the method was verified to be applicable and is expected to have a wide range of applications. The intrinsic redox reaction between LFP and NCM avoids the need for additional oxidants or reductants, while the salt leaching by Fe^{3+} reduces the consumption of strong acids. The synergistic salt leaching method is expected to achieve recycling efficiencies of valuable metals from mixed spent LIB cathodes, with high efficiency, high selectivity and great environmental benefits.

Author contributions

Yunhui Hua: Concept proposed, methodology, formal analysis, data analysis, writing – original draft preparation, formal analysis, and investigation. Zhenghe Xu: Review and editing and methodology. Baojun Zhao: Methodology, review and editing, and supervision. Zuotai Zhang: Concept proposed, methodology, review and editing, supervision, project administration, and funding acquisition.

Conflicts of interest

There are no conflicts to declare.

Acknowledgements

We gratefully acknowledge the Shenzhen Peacock Plan (KQTD20160226195840229) and the support from the Shenzhen Science and Technology Innovation Committee (JCYJ20200109141437586, JCYJ20200109141642225, and JCYJ20200109141227141). We are also grateful to the Guangdong Province Universities and Colleges Pearl River Scholar Funded Scheme 2018.

Notes and references

1 Global EV Outlook 2021 – Analysis – IEA, **https://www.iea.org/reports/global-ev-outlook-2021**, (accessed 13 December 2021).
2 EV-Volumes – The Electric Vehicle World Sales Database, **https://www.ev-volumes.com/country/total-world-plug-in-vehicle-volumes/**, (accessed 13 December 2021).
3 Y. Hua, X. Liu, S. Zhou, Y. Huang, H. Ling and S. Yang, *Resour., Conserv. Recycl.*, 2021, **168**, 105249.
4 M. J. Esfandyari, V. Esfahanian, M. R. H. Yazdi, H. Nehzati and O. Shekoofa, *Energy*, 2019, **176**, 505–520.
5 P. Meshram, A. Mishra, Abhilash and R. Sahu, *Chemosphere*, 2020, **242**, 125291.
6 C. M. Costa, J. C. Barbosa, R. Gonçalves, H. Castro, F. J. D. Campo and S. Lanceros-Méndez, *Energy Storage Mater.*, 2021, **37**, 433–465.
7 M. Shahjalal, P. K. Roy, T. Shams, A. Fly, J. I. Chowdhury, M. R. Ahmed and K. Liu, *Energy*, 2022, **241**, 122881.
8 M. Sethurajan and S. Gaydardzhiev, *Resour., Conserv. Recycl.*, 2021, **165**, 105225.
9 K. M. Winslow, S. J. Laux and T. G. Townsend, *Resour., Conserv. Recycl.*, 2018, **129**, 263–277.
10 G. Harper, R. Sommerville, E. Kendrick, L. Driscoll, P. Slater, R. Stolkin, A. Walton, P. Christensen, O. Heidrich, S. Lambert, A. Abbott, K. Ryder, L. Gaines and P. Anderson, *Nature*, 2019, **575**, 75–86.
11 X. Zhang, L. Li, E. Fan, Q. Xue, Y. Bian, F. Wu and R. Chen, *Chem. Soc. Rev.*, 2018, **47**, 7239–7302.
12 B. Makuza, Q. Tian, X. Guo, K. Chattopadhyay and D. Yu, *J. Power Sources*, 2021, **491**, 229622.
13 E. Fan, L. Li, Z. Wang, J. Lin, Y. Huang, Y. Yao, R. Chen and F. Wu, *Chem. Rev.*, 2020, **120**, 7020–7063.
14 W. Mrozik, M. A. Rajaeifar, O. Heidrich and P. Christensen, *Energy Environ. Sci.*, 2021, **14**, 6099–6121.
15 Y. Yao, M. Zhu, Z. Zhao, B. Tong, Y. Fan and Z. Hua, *ACS Sustainable Chem. Eng.*, 2018, **6**, 13611–13627.
16 R. Wang, Y. Lin and S. Wu, *Hydrometallurgy*, 2009, **99**, 194–201.
17 Z. Takacova, T. Havlik, F. Kukurugya and D. Orac, *Hydrometallurgy*, 2016, **163**, 9–17.
18 L. Sun and K. Qiu, *J. Hazard. Mater.*, 2011, **194**, 378–384.
19 J. Kang, G. Senanayake, J. Sohn and S. M. Shin, *Hydrometallurgy*, 2010, **100**, 168–171.
20 W. Gao, J. Song, H. Cao, X. Lin, X. Zhang, X. Zheng, Y. Zhang and Z. Sun, *J. Cleaner Prod.*, 2018, **178**, 833–845.
21 L. Li, J. Ge, F. Wu, R. Chen, S. Chen and B. Wu, *J. Hazard. Mater.*, 2010, **176**, 288–293.
22 R. Golmohammadzadeh, F. Rashchi and E. Vahidi, *Waste Manage.*, 2017, **64**, 244–254.
23 X. Chen, C. Luo, J. Zhang, J. Kong and T. Zhou, *ACS Sustainable Chem. Eng.*, 2015, **3**, 3104–3113.

24 X. Zhang, Y. Bian, S. Xu, E. Fan, Q. Xue, Y. Guan, F. Wu, L. Li and R. Chen, *ACS Sustainable Chem. Eng.*, 2018, **6**, 5959–5968.
25 X. Zeng, J. Li and B. Shen, *J. Hazard. Mater.*, 2015, **295**, 112–118.
26 Z. Zheng, M. Chen, Q. Wang, Y. Zhang, X. Ma, C. Shen, D. Xu, J. Liu, Y. Liu, P. Gionet, I. O'Connor, L. Pinnell, J. Wang, E. Gratz, R. Arsenault and Y. Wang, *ACS Sustainable Chem. Eng.*, 2018, **6**, 13977–13982.
27 P. Meshram, B. D. Pandey and T. R. Mankhand, *Chem. Eng. J.*, 2015, **281**, 418–427.
28 Y. Hua, Y. Sun, F. Yan, S. Wang, Z. Xu, B. Zhao and Z. Zhang, *Chem. Eng. J.*, 2022, **436**, 133200.
29 H. Li, S. Xing, Y. Liu, F. Li, H. Guo and G. Kuang, *ACS Sustainable Chem. Eng.*, 2017, **5**, 8017–8024.
30 J. Zhang, J. Hu, Y. Liu, Q. Jing, C. Yang, Y. Chen and C. Wang, *ACS Sustainable Chem. Eng.*, 2019, **7**, 5626–5631.
31 T. Tsuneda and T. Taketsugu, *Phys. Chem. Chem. Phys.*, 2018, **20**, 24992–24999.
32 C. M. Lousada, M. Yang, K. Nilsson and M. Jonsson, *J. Mol. Catal. A: Chem.*, 2013, **379**, 178–184.
33 J. Xiao, J. Li and Z. Xu, *Environ. Sci. Technol.*, 2020, **54**, 9–25.
34 J. Li, G. Wang and Z. Xu, *J. Hazard. Mater.*, 2016, **302**, 97–104.
35 W. Wang, Y. Zhang, X. Liu and S. Xu, *ACS Sustainable Chem. Eng.*, 2019, **7**, 12222–12230.
36 F. Liu, C. Peng, A. Porvali, Z. Wang, B. P. Wilson and M. Lundström, *ACS Sustainable Chem. Eng.*, 2019, **7**, 16103–16111.
37 C. Xu, Q. Dai, L. Gaines, M. Hu, A. Tukker and B. Steubing, *Commun. Mater.*, 2020, **1**, 99.
38 Y. Jiang, X. Chen, S. Yan, S. Li and T. Zhou, *Chem. Eng. J.*, 2021, **426**, 131637.
39 Y. Liu, W. Lv, X. Zheng, D. Ruan, Y. Yang, H. Cao and Z. Sun, *ACS Sustainable Chem. Eng.*, 2021, **9**, 3183–3194.
40 E. A. Dalini, G. Karimi, S. Zandevakili and M. Goodarzi, *Miner. Process. Extr. Metall. Rev.*, 2020, **42**, 451–472.
41 Q. Jing, J. Zhang, Y. Liu, C. Yang, B. Ma, Y. Chen and C. Wang, *J. Phys. Chem. C*, 2019, **123**, 14207–14215.
42 J. Kumar, R. R. Neiber, J. Park, R. A. Soomro, G. W. Greene, S. A. Mazari, H. Y. Seo, J. H. Lee, M. Shon, D. W. Chang and K. Y. Cho, *Chem. Eng. J.*, 2022, **431**, 133993.
43 Z. Chen, J. Wang, D. Chao, T. Baikie, L. Bai, S. Chen, Y. Zhao, T. C. Sum, J. Lin and Z. Shen, *Sci. Rep.*, 2016, **6**, 25771.
44 T. Nshizirungu, M. Rana, Y. T. Jo and J. H. Park, *J. Hazard. Mater.*, 2021, **414**, 125575.
45 Y. Yang, G. Huang, M. Xie, S. Xu and Y. He, *Hydrometallurgy*, 2016, **165**, 358–369.
46 X. Jiang, Y. Wei, X. Yu, P. Dong, Y. Zhang, Y. Zhang and J. Liu, *J. Mater. Sci.: Mater. Electron.*, 2018, **29**, 15869–15877.
47 Y. Zhang, W. Wang, Q. Fang and S. Xu, *Waste Manage.*, 2020, **102**, 847–855.
48 J. Li, S. Xiong, Y. Liu, Z. Ju and Y. Qian, *Nano Energy*, 2013, **2**, 1249–1260.
49 Y. Shi, G. Chen, F. Liu, X. Yue and Z. Chen, *ACS Energy Lett.*, 2018, **3**, 1683–1692.
50 L. Yang, Y. Feng, C. Wang, D. Fang, G. Yi, Z. Gao, P. Shao, C. Liu, X. Luo and S. Luo, *Chem. Eng. J.*, 2022, **431**, 133232.
51 H. Zou, E. Gratz, D. Apelian and Y. Wang, *Green Chem.*, 2013, **15**, 1183–1191.
52 W. Lv, Z. Wang, H. Cao, X. Zheng, W. Jin, Y. Zhang and Z. Sun, *Waste Manage.*, 2018, **79**, 545–553.
53 W. Gao, X. Zhang, X. Zheng, X. Lin, H. Cao, Y. Zhang and Z. Sun, *Environ. Sci. Technol.*, 2017, **51**, 1662–1669.
54 Y. Yang, X. Meng, H. Cao, X. Lin, C. Liu, Y. Sun, Y. Zhang and Z. Sun, *Green Chem.*, 2018, **20**, 3121–3133.
55 X. Xiao, B. W. Hoogendoorn, Y. Ma, S. A. Sahadevan, J. M. Gardner, K. Forsberg and R. T. Olsson, *Green Chem.*, 2021, **23**, 8519–8532.
56 J. Kumar, X. Shen, B. Li, H. Liu and J. Zhao, *Waste Manage.*, 2020, **113**, 32–40.
57 L. Li, J. B. Dunn, X. X. Zhang, L. Gaines, R. J. Chen, F. Wu and K. Amine, *J. Power Sources*, 2013, **233**, 180–189.
58 L. Xing, J. Bao, S. Zhou, Y. Qiu, H. Sun, S. Gu and J. Yu, *Chem. Eng. J.*, 2021, **420**, 129593.
59 C. R. Birkl, M. R. Roberts, E. McTurk, P. G. Bruce and D. A. Howey, *J. Power Sources*, 2017, **341**, 373–386.
60 X. Han, L. Lu, Y. Zheng, X. Feng, Z. Li, J. Li and M. Ouyang, *eTransportation*, 2019, **1**, 100005.
61 Y. Qi, F. Meng, X. Yi, J. Shu, M. Chen, Z. Sun, S. Sun and F. Xiu, *J. Cleaner Prod.*, 2020, **251**, 119665.
62 C. Wang, S. Wang, F. Yan, Z. Zhang, X. Shen and Z. Zhang, *Waste Manage.*, 2020, **114**, 253–262.